

## Article

# Experimental Study of the Factors Influencing the Performance of the Bonding Interface between Epoxy Asphalt Concrete Pavement and a Steel Bridge Deck

Zhengxiong Chen <sup>1</sup> , Wei Xu <sup>1,\*</sup> , Jian Zhao <sup>2,\*</sup>, Luming An <sup>2</sup>, Feng Wang <sup>1</sup>, Zizhan Du <sup>1</sup> and Qiang Chen <sup>1</sup>

- <sup>1</sup> School of Civil Engineering and Transportation, South China University of Technology, Guangzhou 510641, China; 201920107290@mail.scut.edu.cn (Z.C.); 202021010287@mail.scut.edu.cn (F.W.); 202121010559@mail.scut.edu.cn (Z.D.); 202121010542@mail.scut.edu.cn (Q.C.)
- <sup>2</sup> China Railway Construction Bridge Engineering Bureau Group Southern Engineering Co., Ltd., Guangzhou 511400, China; anluming@foxmail.com
- \* Correspondence: xuweib@scut.edu.cn (W.X.); zhaojianll@126.com (J.Z.)

**Abstract:** The bonding between pavement and a steel bridge deck is a key component affecting the structural integrity of steel deck pavement and delamination is a major cause. The bonding interface of steel deck pavement was systematically investigated to evaluate the interactive influences of factors, such as the air void of the asphalt concrete pavement, the surface roughness of the steel deck, the thickness of the zinc-rich epoxy primer, and the waterproof bonding membrane, on the bond strength of the pavement interface, through simulated loading, brine immersion, pull-off, and interface observation experiments. The results show that a low air void (<3.0%) was a necessary condition for the corrosion resistance and bonding reliability of the steel deck pavement structure, and a zinc-rich epoxy primer provided an additional guarantee for corrosion resistance of the steel deck pavement; additionally, the combination of steel deck plate roughness in the range of 120–140  $\mu\text{m}$  and zinc-rich epoxy primer thickness in the range of 80–110  $\mu\text{m}$  led to a high bond strength, which was also conducive to the corrosion resistance of the steel bridge plate. The steel deck pavement structure should be designed through combinatorial optimization of multiple factors to create an integrated waterproof and anticorrosion bonding system.

**Keywords:** steel deck pavement; epoxy asphalt concrete; interface; zinc-rich epoxy primer; corrosion resistance; interlayer bonding; roughness; air void



**Citation:** Chen, Z.; Xu, W.; Zhao, J.; An, L.; Wang, F.; Du, Z.; Chen, Q. Experimental Study of the Factors Influencing the Performance of the Bonding Interface between Epoxy Asphalt Concrete Pavement and a Steel Bridge Deck. *Buildings* **2022**, *12*, 477. <https://doi.org/10.3390/buildings12040477>

Academic Editor: Elena Ferretti

Received: 2 March 2022

Accepted: 11 April 2022

Published: 12 April 2022

**Publisher's Note:** MDPI stays neutral with regard to jurisdictional claims in published maps and institutional affiliations.



**Copyright:** © 2022 by the authors. Licensee MDPI, Basel, Switzerland. This article is an open access article distributed under the terms and conditions of the Creative Commons Attribution (CC BY) license (<https://creativecommons.org/licenses/by/4.0/>).

## 1. Introduction

Pavement is laid on the orthotropic steel bridge deck to protect the deck and allow smooth and safe driving of vehicles. A steel deck pavement composite structure is generally composed of a steel deck, an anticorrosion primer, a waterproof bonding membrane (WBM), and the concrete pavement [1,2] (Figure 1). After the steel plate is sandblasted to remove rust, it is generally coated with an anticorrosion primer to prevent it from rusting [3]. Anticorrosive zinc-rich epoxy primers protect the steel deck through the dual action of electrochemical protection and shielding protection and are mostly used in steel deck pavement [4–8]. Studies have shown that the lack or loss of bonding capacity between the orthotropic steel deck and the pavement can directly affect the integrity of the bridge deck pavement, which is mainly manifested as pavement delamination and slippage [9–13].

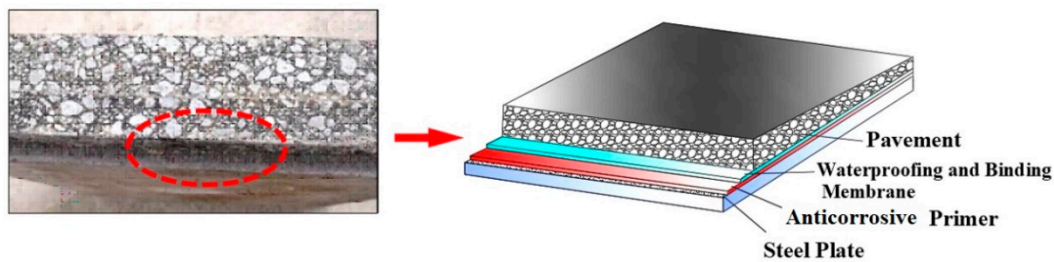


**Figure 1.** Steel deck pavement composite structure.

The field survey of the Humen Bridge in Guangdong Province, China, showed that in areas where the deck pavement and steel deck were well-bonded to each other, the zinc-rich epoxy primer was intact and the steel deck was not corroded (Figure 2), while in areas where delamination between the pavement and the steel deck was observed, moisture enters the interior of the pavement and continuously erodes the steel deck in the wear area of the zinc-rich epoxy primer, causing the steel deck to gradually rust, leading to pavement delamination (Figure 3). The asphalt concrete layer of steel deck pavement should have a low air void to meet the impermeability requirement [14]. Impermeable pavement and bonding with the steel deck are preconditions for steel bridge deck corrosion resistance. Therefore, it is necessary to study in-depth the influencing factors and laws of the corrosion resistance and bonding performance of the pavement bonding interface composed of the pavement asphalt concrete layer, the zinc-rich epoxy primer, the WBM, and the steel deck plate.

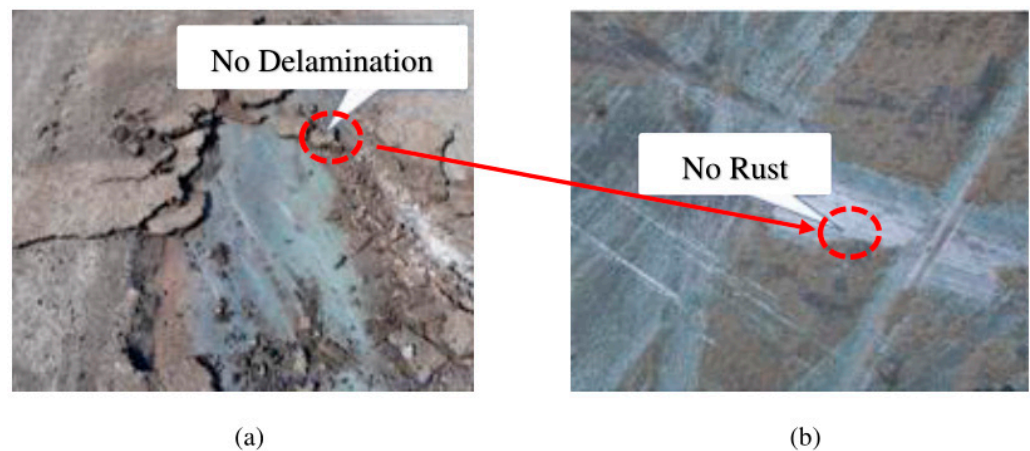


**Figure 2.** An area with good bonding between the deck pavement and the steel deck plate: (a) a well-bonded area; (b) steel plate not rusted.

Chen et al. [15] established a model to predict the behavior of the interface between epoxy asphalt concrete and a composite steel girder subject to a negative bending moment, showing that the physical and mechanical properties of the steel deck and asphalt concrete differ significantly, and that the interface between the steel deck and the asphalt mixture is the weakest in the composite structure. Shen et al. [16] conducted bond strength tests and corrosion tests to show that the bond between the pavement and the anticorrosion primer is gradually damaged and destroyed under repeated fatigue load, resulting in delamination between the pavement and the steel deck. Parhizkar et al. [17] performed electrochemical impedance spectroscopy, pull-off, salt spray, and cathodic delamination tests, revealing that the surface morphology of the epoxy coating affects its adhesion to the steel plate, and that the adhesion is a necessary condition for the anticorrosive properties of the epoxy coating. Knudsen et al. [18] showed through field tests that the larger the thickness of the zinc-rich epoxy primer is, the better its electrochemical properties, which is beneficial in terms of its anticorrosion effect on steel plates. Bocci and Canestrari [19] carried out

comparative tests on the shear properties of smooth and rough steel plate surfaces, showing that the rough steel plate interface has better corrosion resistance, especially at elevated temperatures, than the smooth steel plate. Studies [20–22] have shown that the surface cleanliness and moisture of the steel plate significantly affect the bond strength of the interface between the steel plate and the pavement. Ghumatkar et al. [23] investigated the effect of the bonding surface roughness between mild steel and aluminum on the bond strength, through profile measurements and tensile tests, indicating the existence of an optimal range for the surface roughness of adherend materials. Yan et al. [24] carried out roughness–adhesion, tensile, and corrosion resistance tests, and the test results show that the bond strength between the anticorrosion material and the steel plate is the highest when using a steel plate roughness of 60  $\mu\text{m}$ . In the research outlined above, experimental studies were conducted from perspectives of the steel deck roughness, anticorrosion primer, and environmental factors, showing the existence of an optimal combination of steel plate surface roughness and zinc-rich epoxy primer thickness that results in the highest bond strength between the steel plate and primer. However, there is a lack of systematic research on the influences on the entire steel deck epoxy asphalt pavement structure. At present, there is also a lack of a recommended range for the roughness and zinc-rich epoxy primer thickness in the design of steel deck pavement, and these design parameters are currently generally based on engineering experience.

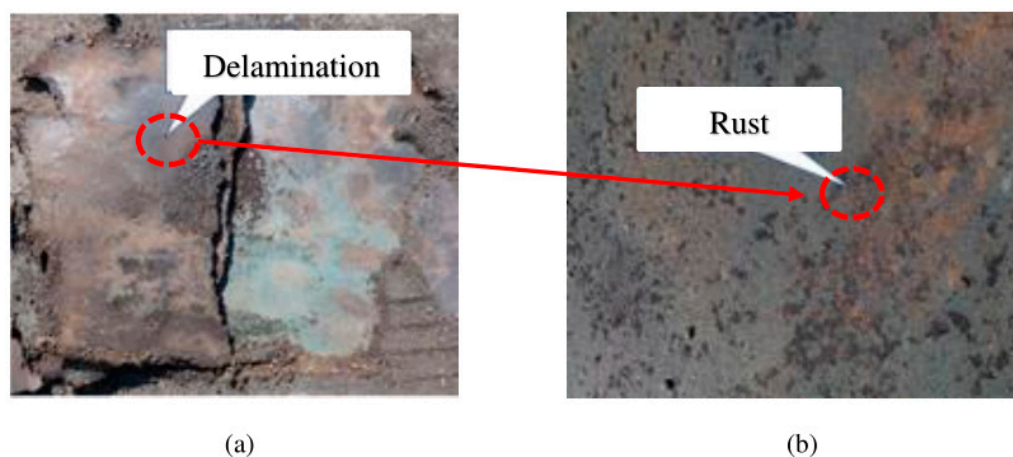


**Figure 3.** An area with delamination between the deck pavement and the steel deck plate: (a) a delaminated area; (b) steel plate rusted.

The bonding interface between the bridge deck pavement and the steel deck is a composite interface composed of the lower pavement surface, the bonding layer, the anticorrosion primer, and the surface of the steel deck, which all interact with each other. At present, the influence of factors, such as pavement air voids, zinc-rich epoxy primer thickness, and steel deck plate roughness, on the corrosion resistance and bonding performance of the steel deck pavement remains unclear. It is necessary to conduct tests to systematically evaluate the influencing factors and laws of the performance of the interface composed of the pavement, bonding layer, zinc-rich epoxy primer, and steel deck surface.

In engineering practice, the zinc-rich epoxy primer is generally used as an anticorrosion primer for epoxy asphalt pavement. However, this is not the case in some projects, mainly those based on the consideration that the pavement alone can play a role in waterproofing and anticorrosion and that the zinc-rich epoxy primer may have a negative impact on the bonding performance of the pavement structure; additionally, the elimination of the zinc-rich epoxy primer simplifies the construction process and shortens the construction period. In view of the impact of the zinc-rich epoxy primer on the steel deck pavement, this study evaluated two types of steel deck pavement composite structures made with hot-mix epoxy asphalt pavement as well as with and without a zinc-rich epoxy primer, respectively, “steel plate + epoxy resin bonding layer + epoxy asphalt concrete” (denoted as

“no-zinc”) and “steel plate + zinc-rich epoxy primer + epoxy resin bonding layer + epoxy asphalt concrete” (denoted as “with-zinc”). The flowchart of the research approach is shown in Figure 4. The effects of vehicle load and moisture erosion were simulated through high-temperature wheel loading and saltwater immersion, respectively, to investigate and evaluate the influencing factors and laws of the steel deck pavement bonding and anticorrosion system and to analyze the design requirements for the integrated steel deck pavement structure system.

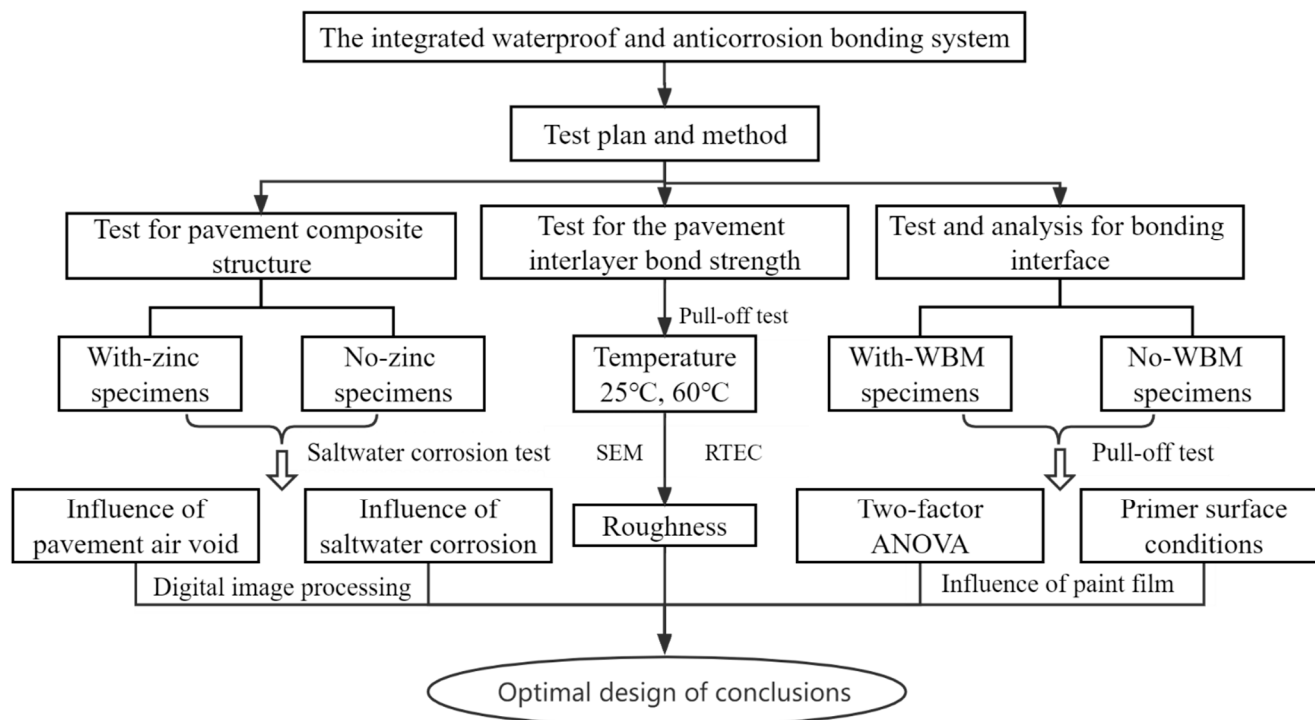


Figure 4. The flowchart of the research approach.

## 2. Materials

### 2.1. Steel Plate

The steel plate was made of Q235 mild steel, and the mechanical properties of the plate are shown in Table 1.

Table 1. Mechanical properties of steel plate material.

Material	Yield Strength (MPa)	Tensile Strength (MPa)	Elastic Modulus (GPa)	Poisson Ratio
Q235 mild steel	235	375–460	200–210	0.3

### 2.2. Zinc-Rich Epoxy Primer

A zinc-rich epoxy primer (Sanhui Paint Co., Ltd., Changshu, Jiangsu, China) was used as the anticorrosion primer for the steel deck, and its material properties are shown in Table 2.

**Table 2.** Material properties of zinc-rich epoxy primer.

Test Item	Unit	Test Result	Test Method [25,26]
Drying time 25 °C	Touch drying	min	16
	Hard drying	h	1.5
Full cure time (25 °C)	h	158	GB/T16777
Tensile adhesion strength (Pull-off test, 25 °C)	MPa	11.6	ASTM D4541

### 2.3. Waterproof Bonding Layer

The waterproof bonding layer was KD-HYP epoxy resin (Kindai Kasei Co., Ltd., Aichi-gun, Aichi-ken, Japan). The technical parameters of the KD-HYP epoxy resin after curing are shown in Table 3.

**Table 3.** Technical parameters of epoxy resin after curing.

Test Item	Unit	Test Result	Test Method [26,27]
Tensile strength (23 °C)	MPa	4.79	ASTM D638
Elongation at break (23 °C)	%	168	ASTM D638
Tensile adhesion strength (25 °C)	MPa	4.04	ASTM D4541
Tensile adhesion strength (60 °C)	MPa	1.96	ASTM D4541

### 2.4. Epoxy Asphalt Concrete

The KD-BEP epoxy asphalt used in the test was a mixture of epoxy resin (Kindai Kasei Co., Ltd., Aichi-gun, Aichi-ken, Japan) and A-70 petroleum matrix asphalt (Shell (China) Co., Ltd., Foshan, Guangdong, China). Epoxy resin components A and B were mixed at a ratio of 56:44, and the resin and A-70 matrix asphalt were mixed at a ratio of 50:50 [28]. The performance parameters of epoxy resins A and B after mixing and curing are shown in Table 4. The performance parameters of the matrix asphalt and epoxy asphalt are shown in Tables 5 and 6, respectively.

**Table 4.** Performance parameters of the epoxy resin.

Test Item	Unit	Test Result	Test Method [27]
Tensile strength at 23 °C	MPa	4.78	ASTM D638
Fracture elongation at 23 °C	%	104	ASTM D638

**Table 5.** Performance parameters of the A-70 matrix asphalt.

Test Item	Unit	Test Result	Test Method [27]
Penetration at 25 °C	0.1 mm	63	ASTM D5
Softening point	°C	47.5	ASTM D36
Ductility at 15 °C, 50 mm/min	cm	>100	ASTM D113
Density at 15 °C	g/cm <sup>3</sup>	1.040	ASTM D1298
Solubility	%	99.80	ASTM D2042
Flash point	°C	337	ASTM D92

**Table 6.** Performance parameters of the epoxy asphalt.

Test Item	Unit	Test Result	Test Method [27]
Penetration at 25 °C	0.1 mm	18	ASTM D5
Softening point	°C	>100	ASTM D36
Tensile strength at 23 °C	MPa	2.91	ASTM D638

The epoxy asphalt mixture was designed using the Marshall test method. The gradation of the epoxy asphalt mixture determined by the test is shown in Table 7 and is

recommended for asphalt layers for steel bridge deck pavements [29]. The gradation curve chart is shown in Figure 5. The optimal asphalt–aggregate ratio was 6.5% according to air void and Marshall stability. The target air void of the epoxy asphalt mixture was controlled by adjusting the compaction level.

**Table 7.** Gradation of the hot-mix epoxy asphalt mixture.

Sieve Size	Percentages (%) of Masses Passing the Following Sieves (Square-Mesh Sieve, mm)								
	13.2	9.5	4.75	2.36	1.18	0.6	0.3	0.15	0.075
Design gradation	100	98.5	76.6	55.2	42.1	31.9	22.5	17.8	12.3
Upper limit	100	100	85	70	55	40	32	23	14
Lower limit	100	95	65	50	39	28	21	14	7

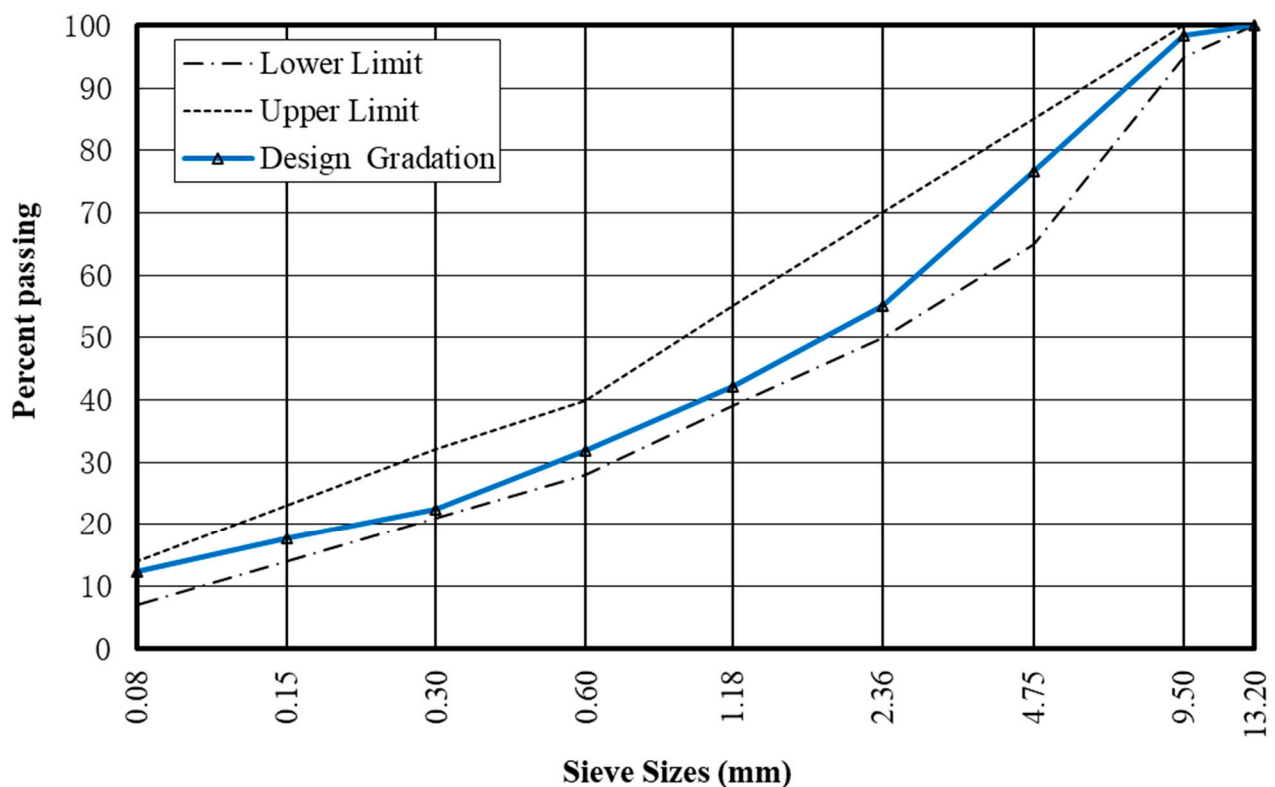


**Figure 5.** The gradation curve chart.

### 3. Test Plan and Method

#### 3.1. Test Plan

##### 3.1.1. Test Plan for Pavement Composite Structure

The hot-mix epoxy asphalt mixture is composed of epoxy asphalt and aggregate, and the designed air void is generally less than 3% [30]. An asphalt mixture air void is a factor affecting moisture infiltration. In general, the permeability of asphalt mixtures can be divided into three types: impermeable, permeable but not drained, and completely drained, which correspond to air void contents of below 5%, 5–20%, and above 20%, respectively [31]. The air void of the asphalt mixture should be controlled within a certain range to prevent the infiltration of moisture [32]. An air void of 2% is generally the target for the compaction control of epoxy asphalt concrete to ensure its impermeability to water [33]. If the epoxy asphalt mixture is insufficiently compacted, the air void is too large, and moisture can easily penetrate, which will cause moisture damage [34–36]. Che et al. evaluated the differences in air voids and permeability before and after dynamic water scouring, showing that an air void of 10% is a critical value of water penetration, beyond which the permeability

coefficient begins to increase and, once new penetration pathways are formed after water scouring, the permeability will increase suddenly [37].

The influences of the air void and saltwater corrosion time of epoxy asphalt concrete on the corrosion resistance and interlayer bonding performance in the with-zinc and no-zinc specimens were evaluated. In this study, the air void of the epoxy asphalt mixture was set to 2% (impermeable), 6% (slightly greater than 5%), and 10% (critical water permeability). The combinations of test parameters are shown in Table 8.

**Table 8.** Combinations of test parameters for pavement composite structure <sup>1</sup>.

Combination No.	Zinc-Rich Epoxy Primer	Pavement Mixture Air Void (%)	Saltwater Immersion Time (Day)
1	Yes	2	0
2	Yes	2	14
3	Yes	2	28
4	Yes	6	14
5	Yes	10	14
6	No	2	0
7	No	2	14
8	No	2	28
9	No	6	14
10	No	10	14

<sup>1</sup> Three samples were collected for each test of each pavement composite structure.

### 3.1.2. Test and Analysis Plan for Bonding Interface

The specimens of the steel deck pavement bonding interface included “steel plate + zinc-rich epoxy primer” specimens (denoted as “no-WBM” (waterproof bonding membrane)) and “steel plate + zinc-rich epoxy primer + WBM” specimens (denoted as “with-WBM”). The steel plate had three roughnesses (A1, A2, and A3), and the primer had five thicknesses (B1, B2, B3, B4, and B5). Table 9 shows the test parameters of steel deck plate roughness and zinc-rich epoxy primer thickness. The parameters of steel plate roughness and primer thickness for no-WBM specimens are shown in Table 9. Two-factor analysis of variance (ANOVA) was performed to evaluate the influences of steel plate roughness and zinc-rich epoxy primer thickness on the bond strength of the no-WBM specimens.

#### (1) No-WBM interface

**Table 9.** The parameters of steel plate roughness and primer thickness.

Roughness Parameter ID	Steel Plate Roughness (µm)	Primer Thickness Parameter ID	Primer Thickness (µm)
		B1	50–80
A1	80–100	B2	80–110
A2	100–120	B3	110–140
A3	120–140	B4	140–170
		B5	170+

Then, the surface corrosion of the no-WBM specimens with different parameters was observed using optical microscopy to evaluate the influences of the steel plate roughness and the zinc-rich epoxy primer thickness on the corrosion resistance of the no-WBM specimens.

#### (2) With-WBM interface

The parameters of steel plate roughness and primer thickness for the with-WBM specimens are shown in Table 9. The influence of the parameters of the steel plate roughness and the zinc-rich epoxy primer thickness on the bond strength of the with-WBM specimens was analyzed and evaluated.

### 3.1.3. Test Plan for the Pavement Interlayer BOND Strength

The influence of the test temperature on the interlayer bonding performance of the with-zinc and no-zinc specimens was evaluated using parameter combinations (2) and (7) in Table 8. Based on the surface roughness of the steel plate specimens, the factors influencing the bond strength between the pavement layers were studied and analyzed.

### 3.1.4. Saltwater Corrosion Test Plan

An erosion test with saltwater is a simulation of the effects of coastal rainwater on steel deck pavement. The saltwater corrosion test includes the loading process and the saltwater immersion process. This test evaluates the corrosion of the steel plate caused by the penetration of moisture into the pavement and especially investigates the influence on the corrosion resistance and bonding performance of the specimen when the pavement concrete has a high air void, and the wheel loading causes damage to the zinc-rich epoxy primer. To simulate the effect of wheel loading and moisture on the steel deck pavement, the prepared with-zinc and no-zinc specimens were first subjected to wheel loading tests and then saltwater immersion tests.

#### (1) Loading test

A rutting test was performed to evaluate the effect of wheel load on the pavement composite structure. The test setup is shown in Figure 6a. The following parameters were used in the test: temperature, 60 °C; wheel loading frequency, 42 times/min; wheel loading pressure, 0.7 MPa; and loading duration, 10 h.

#### (2) Saltwater immersion test



**Figure 6.** Setups for (a) the wheel loading test and (b) the saltwater immersion test.

After the loading test, the pavement composite structures were immersed in saltwater for 0 d, 14 d, and 28 d, as shown in Table 8. The saltwater immersion test was performed at 25 °C using saturated saltwater prepared by adding 36 g of NaCl reagent per 100 mL of distilled water. The saltwater immersion test setup is shown in Figure 6b.

## 3.2. Specimen Preparation

### 3.2.1. With-Zinc and No-Zinc Specimens

The steel plates used for the with-zinc and no-zinc specimens each had dimensions of 290 mm (length) × 290 mm (width) × 16 mm (thickness). The procedure for preparing the with-zinc specimen was as follows:

- (1) The steel plate was sandblasted, and its roughness was measured;
- (2) The steel plate was sprayed with the zinc-rich epoxy primer, and after seven days, the thickness and pull-off strength of the primer were measured.
- (3) The specimen was coated with a KD-HYP epoxy resin bonding layer of 0.4 kg/m<sup>2</sup> and was then held at 25 °C for one day.

- (4) The steel plate specimen was placed in the rutting plate mold, and an epoxy asphalt mixture was compacted into a composite pavement structure specimen with a thickness of 50 mm.

The preparation procedure of the no-zinc specimens was similar to that of the with-zinc specimens, except that step (2) was omitted.

### 3.2.2. No-WBM and with-WBM Specimens

The steel plates used for the no-WBM and with-WBM specimens each had dimensions of 135 mm (length) × 135 mm (width) × 16 mm (thickness). The steel plates had three roughnesses (A1, A2, and A3) and the primer had five thicknesses (B1, B2, B3, B4, and B5). The specific parameters are shown in Table 9.

## 3.3. Measurement Methods

### 3.3.1. Surface Roughness Measurement

The surface roughness of the steel deck plate was measured using an Elcometer 224 surface profile gauge (Elcometer, Manchester, UK).

### 3.3.2. Scanning Electron Microscopy (SEM) Observation

The measurements of the primer thickness on the rough surface had large variations due to the difference in measurement methods. In this study, the precise distribution of the primer thickness was measured using an S3400N scanning electron microscope (Hitachi, Tokyo, Japan).

- (1) The cross-sectional specimen of the steel plate was prepared.
- (2) The heights of the zinc-rich epoxy primer surface and the steel plate surface were measured, and the height difference was calculated as the actual thickness of the zinc-rich epoxy primer.
- (3) The average of the thickness of the zinc-rich epoxy primer was statistically calculated as the representative thickness of the zinc-rich epoxy primer of the specimen (Figure 7).

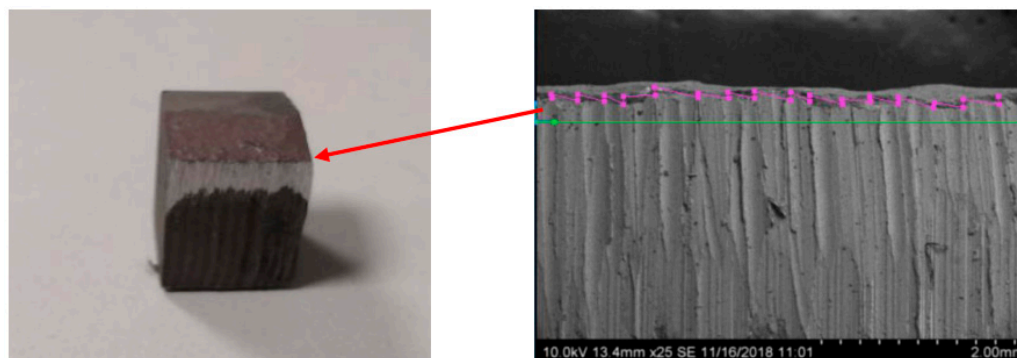


**Figure 7.** Illustration of the SEM measurement of the primer thickness.

### 3.3.3. Confocal Surface Profile Measurement

To reflect the changes in the surface profile of the steel deck plate before and after the application of the zinc-rich epoxy primer, the surface roughnesses of the steel plate and the no-WBM specimen were measured using an RTEC confocal surface profilometer (RTEC Instruments, San Jose, CA, USA), as shown in Figure 8. This profilometer has a measurement accuracy of 0.6  $\mu\text{m}$  and can measure the two-dimensional profile of the specimen and calculate the values of different roughness parameters (the height difference of the surface profile of the steel deck plate).

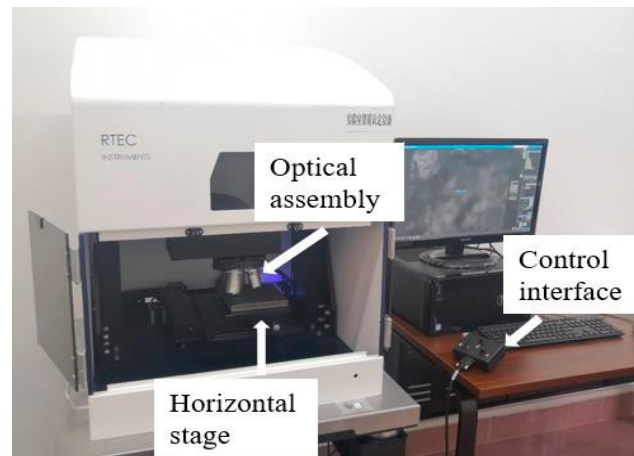


**Figure 8.** RTEC confocal surface profiler.

### 3.3.4. Digital Image Processing of the Steel Plate Corrosion Area

ImageJ is a Java-based image processing software developed by the National Institutes of Health that calculates the pixel counts, spacing, angles, and areas of image regions. ImageJ software was used in this study to calculate the corrosion area of the steel plate surface after saltwater corrosion. The proportion of the corrosion area of the steel plate is calculated by Equation (1) [38]:

$$P = \frac{\sum S}{A_0} \times 100\% \quad (1)$$

where  $P$  is the proportion of the corrosion area of the steel plate (%);  $A_0$  is the total area of the steel plate ( $\text{mm}^2$ ), theoretically  $A_0 = 290 \times 290 = 84,100$  ( $\text{mm}^2$ ); and  $\sum S$  is the total corrosion area of the steel plate after corrosion ( $\text{mm}^2$ ).

### 3.3.5. Pull-Off Test of the Interlayer Bond Strength

The bond strength of the with-zinc and no-zinc specimens was measured using a PosiTest AT-A automatic pull-off testing apparatus (DeFelsko, New York, NY, USA). The test setup is shown in Figure 9a. After the saltwater immersion test, cores were drilled in the wheel track zones of the with-zinc and no-zinc specimens to a depth reaching the surface of the steel plate and with a diameter of 50 mm. A pull-off head with a diameter of 50 mm was glued to the surface of the concrete core.



**Figure 9.** Pull-off test setups for (a) the with-zinc and no-zinc specimens and (b) the no-WBM and with-WBM specimens.

Similarly, the bond strength of the no-WBM and with-WBM specimens was measured using the PosiTest AT-A apparatus (Figure 9b).

## 4. Results and Discussion

### 4.1. Pavement Interlayer Bonding Performance

The failure modes of the with-zinc and no-zinc specimens in the pull-off test were divided into the internal fracture of the concrete and the interfacial fracture of the bonding layer, as shown in Figure 10a,b, respectively.



**Figure 10.** Interface states of specimen failure in the pull-off test: (a) the internal fracture of the concrete and (b) the interfacial fracture of the bonding layer.

The influence of the temperature on the interlayer bond strength of the with-zinc and no-zinc specimens was evaluated using parameter combinations (2) and (7) in Table 8. The test analysis data are shown in Figure 11. At the test temperature of 25 °C, the failure modes of the with-zinc and no-zinc specimens were “internal fracture of the concrete,” corresponding to the failure strengths of 2.63 MPa and 2.75 MPa, respectively, as shown in Figure 11. The error bars illustrate standard deviation (SD) of the measured data in Figure 11, and it shows that the test data are relatively uniform. At a test temperature of 60 °C, the failure modes of the with-zinc and no-zinc specimens showed both “internal fracture of the concrete” and “interfacial fracture of the bonding layer,” with an insignificant difference in strength. The proportions of specimens with each failure mode are shown in Table 10. In particular, the proportions of the with-zinc and no-zinc specimens with the failure mode of “interfacial fracture of the bonding layer” were 37.5% and 12.5%, respectively, as shown in Table 10. As the temperature increased from 25 °C to 60 °C, the bond strength of the bonding layer interface was significantly reduced compared to that of the epoxy asphalt concrete; hence, the pavement structure fractured at the relatively weak part in the pull-off test.

The analysis of data in Table 10 reveals that at the test temperature of 60 °C, 37.5% of the with-zinc specimens and 12.5% of the no-zinc specimens fractured at the interface of the bonding layer, indicating that fracture mainly occurred in the concrete during the pull-off test.

Dam et al. [39] found that the increase in the surface roughness of a steel plate is conducive to increasing the bonding area of the bonding interface, thereby improving the adhesion of the bonding layer. However, pavement parts were not included in their study.

A comparison of the roughness of the no-zinc and with-zinc specimens showed that the surface roughness of the with-zinc specimens, which were sprayed with zinc-rich epoxy primer, was reduced by an average of 23.7% compared to that of the no-zinc steel plate, as shown in Figure 12. The overall height difference of the profile of the with-zinc specimens was significantly smaller than that of the surface structure of the no-zinc steel plate, as shown in Figure 13. The curves in Figure 13 are the averaged results from the surface profile measurements. Due to the viscosity and spray unevenness of epoxy zinc-rich, it will locally accumulate into peaks and valleys in the curves in Figure 13. These results indicate that the spraying of zinc-rich epoxy primer on the steel deck plate reduced the surface roughness and decreased the bonding area of the bonding interface. However, the comparison of the test data of the with-zinc and no-zinc specimens showed that for the pavement composite

structure, the difference in the interlayer bond strength with and without the zinc-rich epoxy primer was not significant, indicating that the zinc-rich epoxy primer had no significant influence on the bond strength of the pavement composite structure.

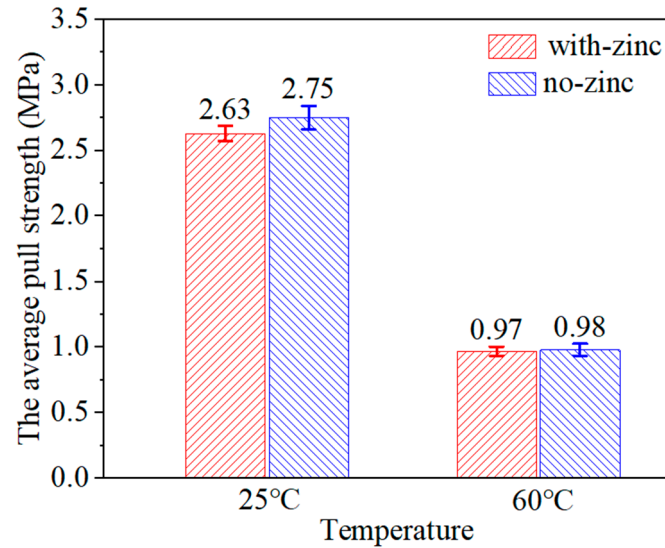


Figure 11. Influences of temperature and zinc primer on the interlayer bond strength.

Table 10. Statistics of the failure modes of the with-zinc and no-zinc specimens<sup>1</sup> (at 60 °C).

Specimen Type	Number of Specimens with Internal Fracture of the Concrete	Proportion	Number of Specimens with Interfacial Fracture of the Bonding Layer	Proportion
with-zinc	5	62.5%	3	37.5%
no-zinc	7	87.5%	1	12.5%

<sup>1</sup> There were eight specimens in each of the with-zinc and no-zinc specimen groups for the pull-off tests. The failure modes of both the with-zinc and no-zinc specimens were the “internal fracture of the concrete” at a temperature of 25 °C.

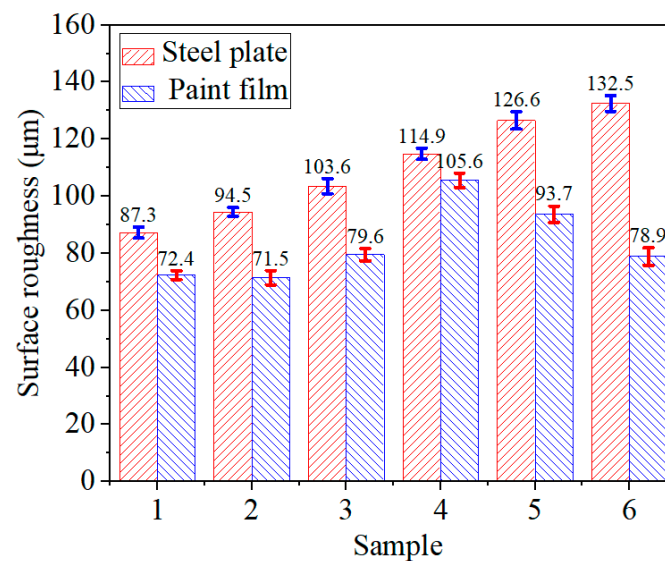
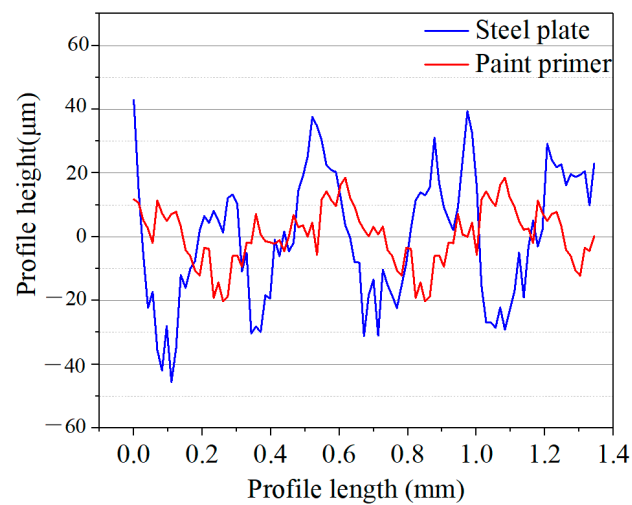


Figure 12. Comparison of the surface roughness of the steel plate and the primer. (Samples 1–6 are a series of samples with a roughness range of 80–150 µm).



**Figure 13.** Comparison of the profiles of the steel plate surface without and with primer spray.

#### 4.2. Analysis of the Bonding Interface

##### 4.2.1. No-WBM Bonding Interface

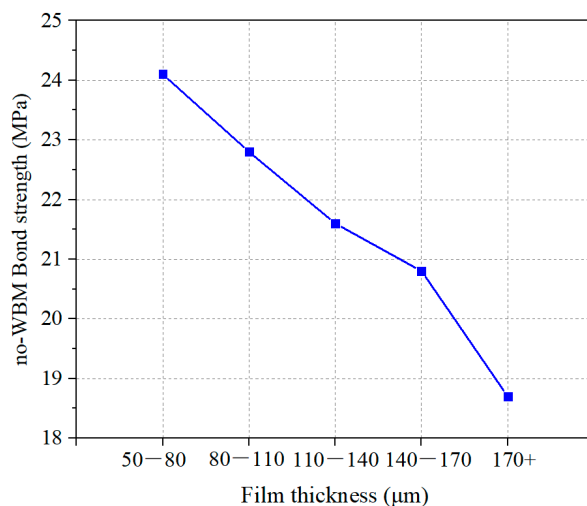
The bond strength of the no-WBM specimens (denoted as “no-WBM bond strength”) was measured using the PosiTest AT-A apparatus. The measurement data are shown in Table 11. The results of two-factor ANOVA of no-WBM bond strength are shown in Table 12. Significant probability of statistics (Sig.) for film thickness was 0.025 (<0.05), indicating that the thickness of epoxy zinc-rich paint film had a significant effect on the bond strength of no-WBM [40]. Table 11 shows the results obtained by repeating the pull test several times. The value of no-WBM sample 12 was significantly different, because the combination of “A3 + B2” is prone to test errors without the waterproof adhesive layer. A two-factor ANOVA showed that the no-WBM bond strength decreased with the increase in the thickness of the zinc-rich epoxy primer (Figure 14). The no-WBM bond strength was the highest when the zinc-rich epoxy primer was 50–80 µm thick. This result indicates that at a given steel plate roughness and within the range of the primer thickness in this study, a smaller zinc-rich epoxy primer thickness was more beneficial for the no-WBM bond strength.

**Table 11.** Bond strength of the no-WBM specimens.

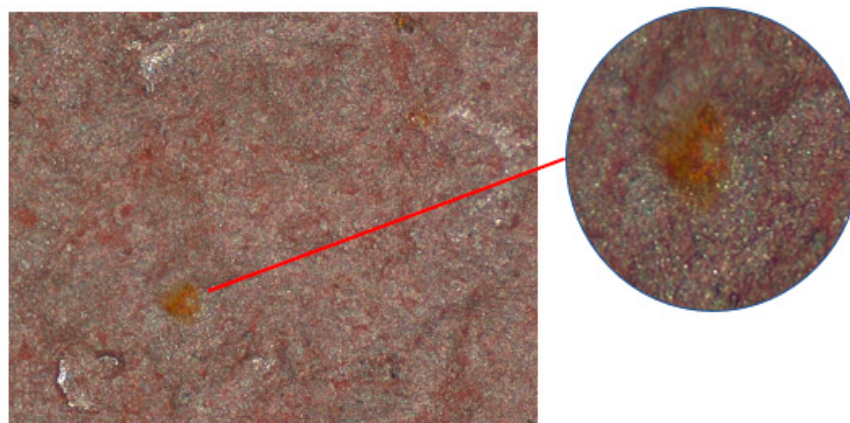
Specimens No.	Steel Plate Roughness (µm)	Primer Thickness (µm)	No-WBM Bond Strength (MPa)			
1	A1	B1	24.0	24.0	24.0	24.0
2	A1	B2	24.0	24.0	24.0	24.0
3	A1	B3	19.5	21.6	22.6	24.0
4	A1	B4	18.0	15.4	19.6	24.0
5	A1	B5	18.2	18.7	17.6	19.2
6	A2	B1	24.0	23.6	23.8	23.2
7	A2	B2	22.7	21.6	18.9	23.2
8	A2	B3	24.0	21.9	23.2	18.6
9	A2	B4	24.0	24.0	20.8	20.9
10	A2	B5	19.6	18.5	20.3	17.4
11	A3	B1	23.5	24.0	24.0	22.9
12	A3	B2	19.9	21.5	23.4	23.8
13	A3	B3	20.2	21.4	22.6	22.8
14	A3	B4	20.6	21.5	20.6	22.2
15	A3	B5	19.3	20.6	20.3	22.9

**Table 12.** Results of two-factor ANOVA of no-WBM bond strength.

Variance Source	Sum of Squares	Degree of Freedom	Average Square	Sig.
Steel plate roughness	1.527	2	0.764	0.878
Film thickness	76.098	4	19.024	0.025

**Figure 14.** Relationship between the primer thickness and bond strength.

The corrosion resistance of the primer surface of the no-WBM specimens with different steel plate roughnesses was observed using optical microscopy (Figures 15–17). Table 13 gives the data showing the influences of steel plate roughness and primer thickness on the corrosion of the primer surface of the no-WBM specimens. Statistically, the thickness of epoxy-rich zinc primer was the main factor influencing the anticorrosive performance of the steel plate. The surface of the no-WBM specimen was susceptible to corrosion when the zinc-rich epoxy primer had a thickness of 50–80 µm. In comparison, the surface of the no-WBM specimen was rust- and crack-free when the zinc-rich epoxy primer was 80–170 µm thick. The surface of the no-WBM specimen was prone to cracks when the thickness of the zinc-rich epoxy primer was greater than 170 µm. The relationship between the primer thickness and the corrosion condition within the range of the primer thickness considered in this study showed that a thinner zinc-rich epoxy primer (50–80 µm) was not conducive to the corrosion resistance of the steel plate and resulted in corrosion, while a thicker zinc-rich epoxy primer (170+ µm) was not conducive to the integrity of the primer, and the surface was susceptible to cracking. Based on the test data, the thickness of the zinc-rich epoxy primer should be in the range of 80–170 µm.

**Figure 15.** Rust spots on the surface of the no-WBM specimen with a primer thickness of 50–80 µm.

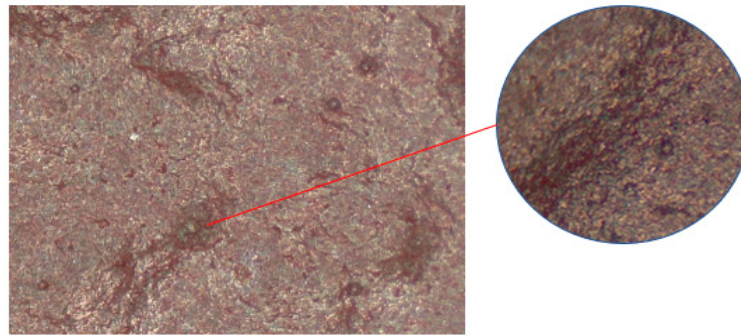


**Figure 16.** No rust spot or cracks on the surface of the no-WBM specimen with a primer thickness of 80–170  $\mu\text{m}$ .

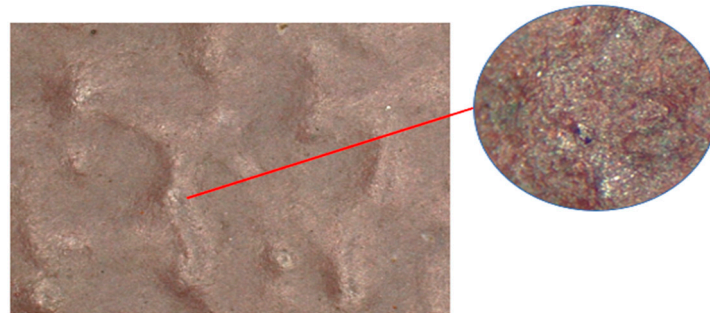


**Figure 17.** Cracks on the surface of the no-WBM specimen with a primer thickness of 170+  $\mu\text{m}$ .

**Table 13.** Primer surface conditions of the no-WBM specimens.

Specimens No.	Steel Plate Roughness ( $\mu\text{m}$ )	Primer Thickness ( $\mu\text{m}$ )	Condition of the Primer Surface
1	80–100	50–80	Rust spots
2	80–100	80–110	No rust, no cracks
3	80–100	110–140	No rust, no cracks
4	80–100	140–170	No rust, no cracks
5	80–100	170+	Cracks
6	100–120	50–80	Rust spots
7	100–120	80–110	No rust, no cracks
8	100–120	110–140	No rust, no cracks
9	100–120	140–170	No rust, no crack
10	100–120	170+	Cracks
11	120–140	50–80	Rust spots
12	120–140	80–110	No rust, no cracks
13	120–140	110–140	No rust, no cracks
14	120–140	140–170	No rust, no cracks
15	120–140	170+	Cracks

#### 4.2.2. With-WBM Bonding Interface

The bond strength of the with-WBM specimens (denoted as “with-WBM bond strength”) was measured using the PosiTest AT-A pull-off apparatus (Table 14). A two-factor ANOVA was performed on the with-WBM bond strength data in Table 14, with the results shown in Figure 18. The results of two-factor ANOVA of with-WBM bond strength are shown in Table 15. In the two-factor ANOVA, the steel plate roughness and zinc-rich epoxy primer thickness had statistical significance (Sig.) of 0.030 and 0.001 (both  $<0.05$ ), respectively, indicating that both parameters had a significant influence on the with-WBM bond strength. The with-WBM bond strength increased as the surface roughness of the steel plate increased. In comparison, as the thickness of the zinc-rich epoxy primer increased, the with-WBM bond strength tended to first increase and then decrease. The with-WBM bond strength

corresponding to a zinc-rich epoxy primer thickness of 50–80  $\mu\text{m}$  was lower than that corresponding to a primer thickness of 80–110  $\mu\text{m}$ . This is because specimens with a thinner primer were more prone to rusting, as shown in Figure 15, causing delamination between the primers and decreasing the with-WBM bond strength. In comparison, the with-WBM specimens with a thicker zinc-rich epoxy primer (170+  $\mu\text{m}$ ) had a lower bond strength. This is because an excessively thick primer easily led to the cracking of the with-WBM specimens (Figure 17), which was not conducive to interlayer bonding. On the one hand, an analysis of Figure 18 and Table 13 reveals that when the thickness of the zinc-rich epoxy primer was 80–110  $\mu\text{m}$ , the with-WBM specimen had a relatively large bond strength, and there was no rust or cracks on the surface of the primer of this thickness, which was beneficial for the protection of the steel plate. On the other hand, a steel plate surface roughness of 120–140  $\mu\text{m}$  enabled the formation of a large surface bonding area, which was conducive to interlayer bonding. Overall, the with-WBM specimen had a high bond strength and good corrosion resistance when the steel plate roughness was 120–140  $\mu\text{m}$  and the zinc-rich epoxy primer thickness was 80–110  $\mu\text{m}$ .

**Table 14.** Bond strengths of the with-WBM specimens.

Specimens No.	Steel Plate Roughness ( $\mu\text{m}$ )	Primer Thickness ( $\mu\text{m}$ )	With-WBM Bond Strength (MPa)			
1	A1	B1	7.2	6.7	6.8	7.3
2	A1	B2	7.8	7.1	7.2	7.6
3	A1	B3	5.9	7.4	5.6	6.5
4	A1	B4	6.2	6.5	6.1	6.1
5	A1	B5	5.8	6.0	5.6	4.8
6	A2	B1	7.4	6.9	7.2	6.6
7	A2	B2	6.5	7.7	8.5	7.6
8	A2	B3	7.5	6.4	7.4	7.6
9	A2	B4	6.8	6.5	7.7	6.6
10	A2	B5	6.6	5.9	6.3	6.7
11	A3	B1	7.7	7.8	7.9	8.2
12	A3	B2	7.8	8.3	7.9	8.5
13	A3	B3	7.6	7.0	7.2	7.8
14	A3	B4	7.3	6.8	7.5	7.2
15	A3	B5	5.9	6.1	6.6	7.8

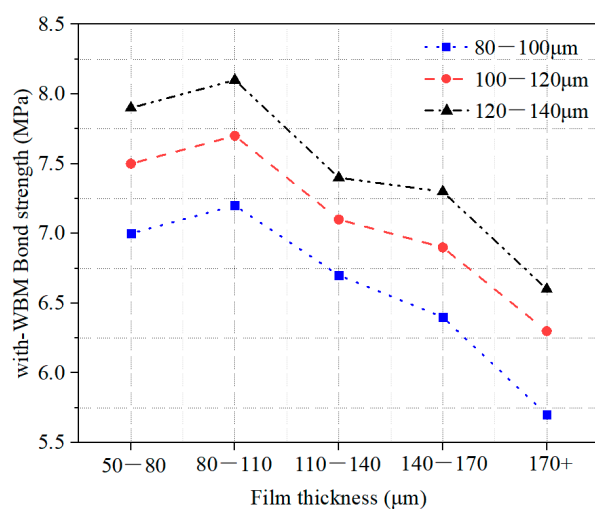


**Figure 18.** Influences of the steel plate roughness and zinc-rich epoxy primer thickness on the with-WBM bond strength.

**Table 15.** Results of two-factor ANOVA of no-WBM bond strength.

Variance Source	Sum of Squares	Degree of Freedom	Average Square	Sig.
Steel plate roughness	2.695	2	1.348	0.030
Film thickness	8.887	4	2.222	0.001

#### 4.3. Composition and Influencing Factors of the Pavement Anticorrosion System

##### 4.3.1. Influence of Pavement Air Void

The test data corresponding to parameter combinations (2), (4), and (5) in Table 8 were comparatively analyzed to evaluate the corrosion resistance of the with-zinc specimens. The steel plates of specimens with air voids of 2% had no corrosion area, as shown in Figure 19a,b. The corrosion resistance of the with-zinc specimen with air voids of 10% was basically the same as that of the with-zinc specimen with air voids of 2%, indicating that the zinc-rich epoxy primer could prevent the corrosion of the steel plate in the case of saltwater entering the pavement. The test data corresponding to parameter combinations (7), (9), and (10) in Table 8 were compared to evaluate the corrosion resistance of the no-zinc specimens, with the test results shown in Figures 19b and 20a. When the concrete had air voids of 2%, the corners of the steel plates were severely corroded. When the air voids of the concrete were 6% and 10%, the overall surface of the steel plate was corroded. As the concrete air voids increased from 2% to 6% and 10%, the proportion of the corrosion area of the steel plate of the no-zinc specimen increased by 3.01- and 3.87-fold, respectively, as shown in Figure 21, indicating that the steel plate of the no-zinc specimen was corroded when the air voids of the pavement were too large (>3%). In addition, during the compaction process of the test, some aggregates wore through the waterproof bonding layer and the zinc-rich epoxy primer to reach the surface of the steel plate, as shown in Figure 22. In this case, moisture penetrated the pavement and reached the surface of the steel plate, resulting in corrosion of the steel deck plate. Therefore, the low air void (<3%) of the epoxy asphalt concrete layer is a precondition for the corrosion resistance of the steel deck pavement.

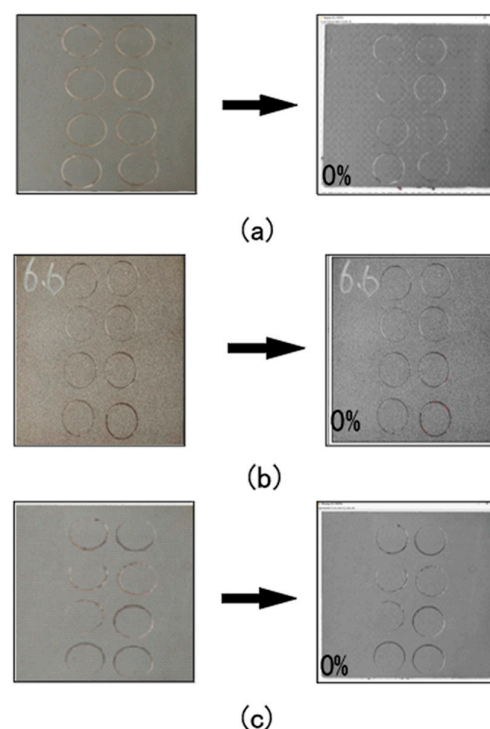


**Figure 19.** Corrosion of the with-zinc specimens with pavement air voids of (a) 2%, (b) 6%, and (c) 10% (Note: the red area represents the corrosion area).

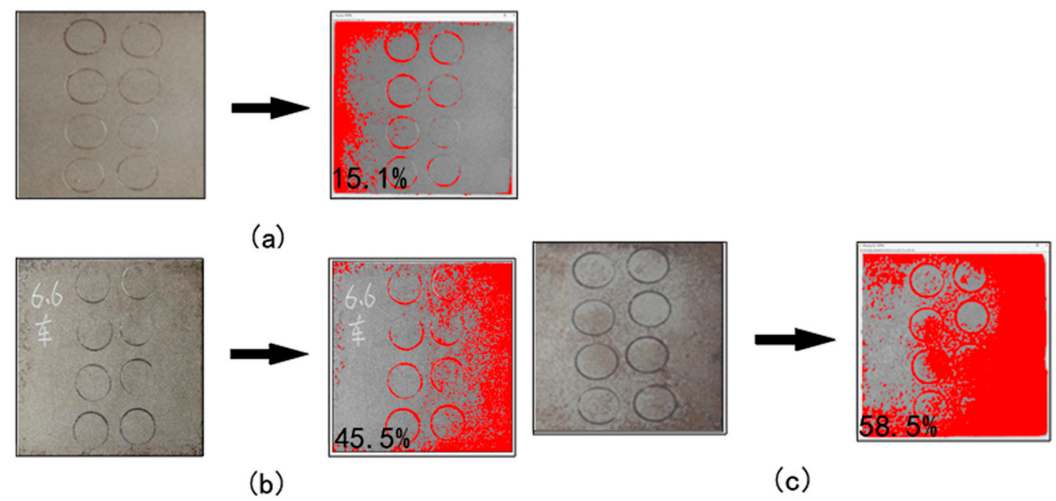


**Figure 20.** Corrosion of the no-zinc specimens with pavement air voids of (a) 2%, (b) 6%, the Chinese character “车” is the meaning of vehicle, and (c) 10% (Note: the red area represents the corrosion area, and the value is the proportion of the corrosion area).

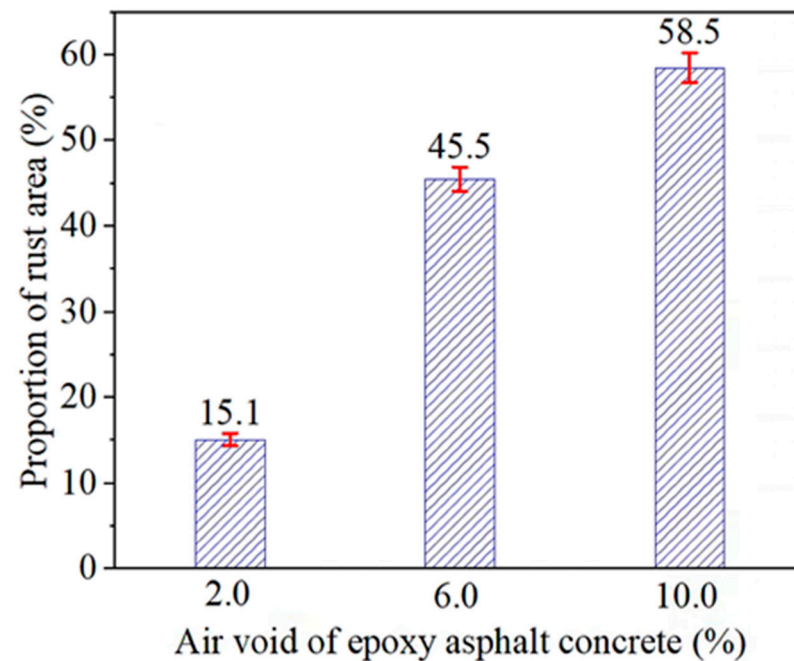


**Figure 21.** Influence of the pavement concrete air void on the corrosion of the steel plate of the composite structure specimen.

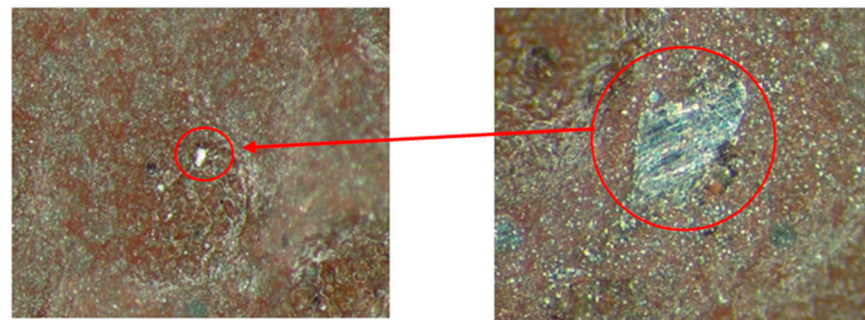


**Figure 22.** During the compaction process, aggregates wore through the zinc-rich epoxy primer and the waterproof bonding layer to reach the steel plate.

The analysis above reveals that, on the one hand, the low air void (<3%) of the pavement concrete was the basis of the steel deck pavement system corrosion resistance, and on the other hand, the presence of the anticorrosion zinc-rich epoxy primer layer provided an additional guarantee for the corrosion resistance of the steel deck pavement. When the air void of the epoxy asphalt concrete was too large (>3%), the with-zinc composite pavement structure could prevent steel plate corrosion to a certain extent. However, the zinc-rich epoxy primer alone could not provide long-term corrosion protection, and the pavement aggregate could gradually wear out the zinc-rich epoxy primer. Therefore, it is necessary to achieve the bonding, waterproofing, and anticorrosion of the steel deck pavement as a whole.

#### 4.3.2. Influence of Saltwater Corrosion

The influence of saltwater corrosion time on the with-zinc specimens was evaluated through a comparative analysis of test data corresponding to parameter combinations (1), (2), and (3) in Table 8. With an increase in the saltwater corrosion time, the proportion of the corrosion area of the steel plate of the with-zinc specimen increased somewhat (0.9%), indicating that the zinc-rich epoxy primer could protect the steel deck plate in the case of saltwater corrosion (Figure 23a,b). The corrosion was attributed to the wearing-through phenomenon shown in Figure 22. The influence of the saltwater corrosion time on the no-zinc specimens was analyzed by comparing the test data corresponding to parameter combinations (6), (7), and (8). The steel plates were not corroded in the absence of saltwater corrosion. After saltwater corrosion for 14 days and 28 days, the proportion of the corrosion area was 45.9% and 48.8%, respectively, and the overall steel plates were corroded, with the results shown in Figure 24a,b and Table 16. Based on the above analysis, when the saltwater corrosion time exceeded 14 days, the with-zinc specimens could protect the steel plate well, while the no-zinc specimens exhibited severe corrosion, indicating that the zinc-rich epoxy primer could protect the steel deck plate to a certain extent.

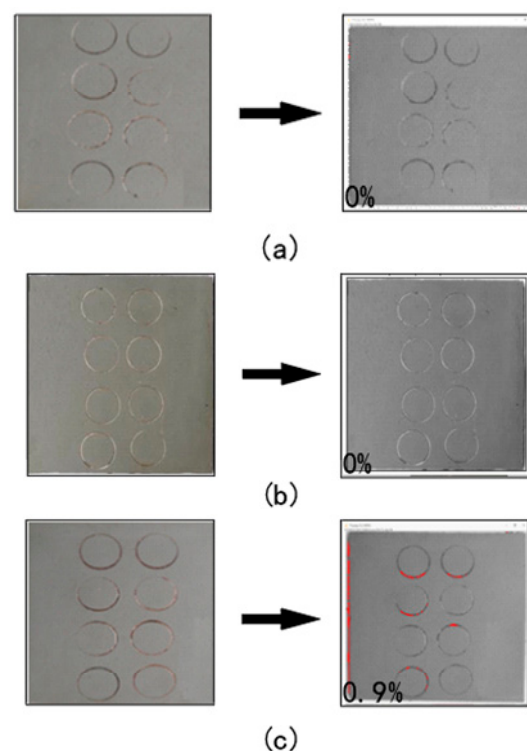


**Figure 23.** Corrosion of the with-zinc specimens after saltwater corrosion for (a) 0 days, (b) 14 days, and (c) 28 days (Note: the red area represents the corrosion area).

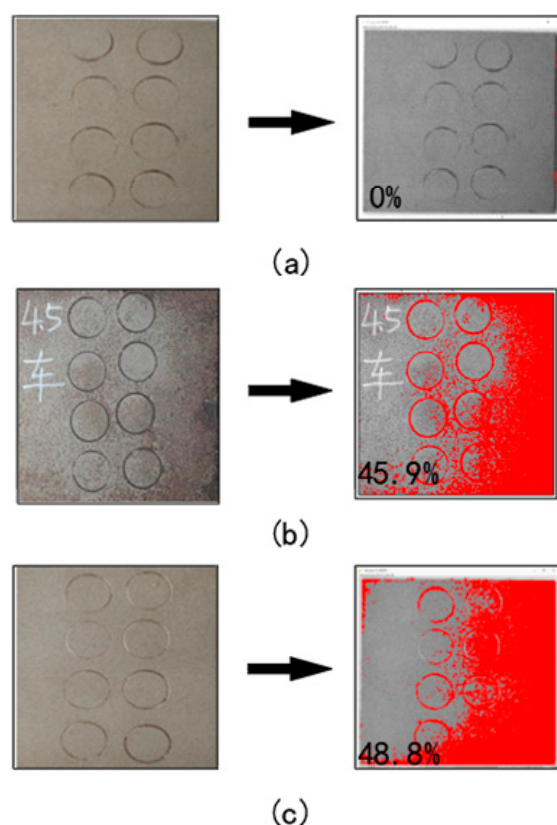


**Figure 24.** Corrosion of the no-zinc specimens after saltwater corrosion for (a) 0 days, (b) 14 days, the Chinese character “车” is the meaning of vehicle, and (c) 28 days (Note: the red area represents the corrosion area, and the value is the proportion of the corrosion area).

**Table 16.** Influence of the saltwater corrosion time on the corrosion of the no-zinc steel plate specimens.

Saltwater Immersion Time (d)	Proportion of Corrosion Area (%)	Corrosion Condition
0	0	No corrosion
14	45.9	Overall corrosion
28	48.8	Overall corrosion

#### 4.4. Optimal Design of a Steel Deck Pavement Structure

The pavement on a steel deck is the main foundation and precondition of the basic barrier against moisture. Epoxy asphalt concrete should be designed with a low air void (<3% as a general requirement), and this research showed that air voids of 2% lead to a satisfactory waterproofing and anticorrosion effect. In addition, the bond strength between the zinc-rich epoxy primer and the steel plate (12.9–24 MPa) was significantly higher than the bond strength of the waterproof bonding layer (5.9–8.5 MPa). Hence, the influence of the combination of the steel plate roughness and the zinc-rich epoxy primer thickness on the bond strength of the epoxy resin waterproof bonding layer can be mainly considered. The with-WBM specimens had a high bond strength and a satisfactory corrosion resistance when the steel plate roughness was 120–140  $\mu\text{m}$  and the zinc-rich epoxy primer thickness was 80–110  $\mu\text{m}$ , and this recommended parameters range is not only conducive to the corrosion resistance of the steel deck pavement but also beneficial for the interlayer bonding performance (Figure 25).

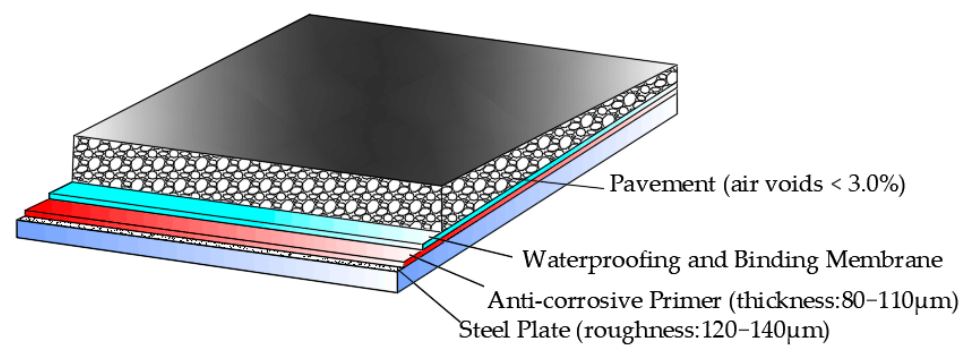


**Figure 25.** Optimal design of a steel deck pavement structure.

## 5. Conclusions

The effects of wheel load and moisture on the epoxy asphalt concrete pavement on steel bridge decks were simulated to evaluate the influencing factors and patterns of the bonding and anticorrosion interface of the steel deck pavement structure. The following conclusions were drawn:

- (1) The pavement structure fractured at its weak position in the pull-off test, and hence, it is necessary to consider the overall coordination of the bond strengths of different layers of the pavement structure. When the temperature of the pull-off test increased from 25 °C to 60 °C, an increasing number of fractures occurred at the interface of the bonding layer. This is because the bond strength of the bonding layer interface was significantly reduced compared to that of the epoxy asphalt concrete due to the increase in temperature. Therefore, attention should be paid to improving the high-temperature performance of the bonding layer to ensure the overall interlayer bonding performance of the steel deck pavement is consistent.
- (2) Under a certain steel plate surface roughness and zinc-rich epoxy primer thickness, the zinc-rich epoxy primer reduced the surface area of the steel deck plate surface structure but had no significant impact on the bond strength of the pavement composite structure. The zinc-rich epoxy primer enhanced the protection of the steel deck plate. Tests showed that the zinc-rich epoxy primer with a thickness of 80–110 μm had a good combined effect of bonding and anticorrosion.
- (3) Under a combination of the three factors (i.e., concrete air void <3%, steel plate roughness of 120–140 μm, and zinc-rich epoxy primer thickness of 80–110 μm), the steel deck pavement structure had a high bond strength and a high corrosion resistance, which are conducive to preventing the problems of pavement delamination and steel deck plate corrosion.
- (4) The pavement, bonding layer, zinc-rich epoxy primer, and steel plate surface roughness form a unified system for the waterproofing, anticorrosion, and bonding of the steel deck pavement structure and, hence, should be designed in a holistic and coordinated manner. The low air void provides a basis for the waterproofing and anticorrosion of the steel deck pavement, the bonding between the pavement and the steel deck is the precondition for the corrosion resistance of the steel deck plate, and the epoxy zinc-rich primer anticorrosion primer offers an additional guarantee for the corrosion performance of the steel deck pavement. In order to confirm the results and ensure a more comprehensive assessment of the analyzed variants, field tests should be carried out under real conditions over a longer period of time.

**Author Contributions:** Conceptualization, W.X. and J.Z.; methodology, W.X.; software, F.W. and Q.C.; investigation, Z.C. and L.A.; resources, L.A. and Z.D.; writing—original draft preparation, W.X. and Z.C.; writing—review and editing, W.X. and J.Z. All authors have read and agreed to the published version of the manuscript.

**Funding:** This research was funded by the National Natural Science Foundation of China, grant No. 51508204; Guangdong Basic and Applied Basic Research Foundation, grant No. 2021A1515011788 in China; the Open Fund Project of the Key Laboratory of Highway Engineering of the Ministry of Education, Changsha University of Science and Technology, grant No. kfj190201, in China; and the Guangdong University Characteristic Innovation Project, grant No. 2020KTSCX009 in China. The support is gratefully acknowledged. The opinions and conclusions presented in this paper are those of the authors and do not necessarily reflect the views of the sponsoring organizations.

**Institutional Review Board Statement:** Not applicable.

**Informed Consent Statement:** Not applicable.

**Data Availability Statement:** Not applicable.

**Conflicts of Interest:** The authors declare no conflict of interest.

## References

1. Huang, Q.; Qian, Z.; Chen, L.; Zhang, M. Evaluation of epoxy asphalt rubber with silane coupling agent used as tack coat for seasonally frozen orthotropic steel bridge decks. *Constr. Build. Mater.* **2019**, *241*, 117957. [[CrossRef](#)]
2. Wang, J.; Xiao, F.; Chen, Z.; Li, X. Application of tack coat in pavement engineering. *Constr. Build. Mater.* **2017**, *152*, 856–871. [[CrossRef](#)]
3. Ministry of Transport of People’s Republic of China. *Specifications for Design and Construction of Pavement on Highway Steel Bridge (JTGT3364-02-2019)*; People’s Communication Press: Beijing, China, 2019. (In Chinese)
4. Jagtap, R.N.; Rakesh, N.; Hassanand, S.Z.; Malshe, V.C. Predictive power for life and residual life of the zinc rich primer coatings with electrical measurement. *Prog. Org. Coat.* **2007**, *58*, 253–258. [[CrossRef](#)]
5. Jagtap, R.N.; Patil, P.; Hassan, S.Z. Effect of zinc oxide in combating corrosion in zinc-rich primer. *Prog. Org. Coat.* **2008**, *63*, 389–394. [[CrossRef](#)]
6. Abreu, C.M.; Izquierdo, M.; Keddani, M.; Nóvoa, X.R.; Takenouti, H. Electrochemical behaviour of zinc-rich epoxy paints in 3% NaCl solution. *Electrochim. Acta* **1996**, *41*, 2405–2415. [[CrossRef](#)]
7. Liu, X.; Xiong, J.; Lv, Y.; Zuo, Y. Study on corrosion electrochemical behavior of several different coating systems by EIS. *Prog. Org. Coat.* **2009**, *64*, 497–503. [[CrossRef](#)]
8. Bera, S.; Rout, T.K.; Udayabhanu, G.; Narayan, J. Water-based & eco-friendly epoxy-silane hybrid coating for enhanced corrosion protection & adhesion on galvanized steel. *Prog. Org. Coat.* **2016**, *101*, 24–44.
9. Medani, T.O.; Liu, X.; Huurman, M.; Scarpas, A. Characterisation of surfacing materials for orthotropic steel deck bridges. Part 1: Experimental work. *Int. J. Pavement Eng.* **2010**, *11*, 237–253. [[CrossRef](#)]
10. Liu, X.; Medani, T.O.; Scarpas, A.; Huurman, M. Characterisation of surfacing materials for orthotropic steel deck bridges. Part 2: Numerical work. *Int. J. Pavement Eng.* **2010**, *11*, 255–265. [[CrossRef](#)]
11. András, G.; Bertóti, I.; Török, T.; Pfeifer, É.; Kálmán, E. Corrosion protection with zinc-rich epoxy paint coatings embedded with various amounts of highly dispersed polypyrrole-deposited alumina monohydrate particles. *Prog. Org. Coat.* **2013**, *76*, 17–32.
12. Luo, S.; Qian, Z.; Wang, H. Condition survey and analysis of epoxy asphalt concrete pavement on Second Nanjing Yangtze River Bridge. *J. Southeast. Univ.* **2011**, *27*, 417–422.
13. Chen, X.H.; Huang, W.; Wang, J.W.; Cheng, G. Damage causes of mastic asphalt pavement on orthotropic steel deck plate. *J. Traf. Transp. Eng.* **2004**, *4*, 5–9.
14. Gaul, R.W.; Seim, C. Epoxy Asphalt Concrete: A Polymer Concrete with 25 Years Experience. American Concrete Institute Technical Session. *Polym. Con. Over.* **1993**, *166*, 233–252.
15. Chen, X.H.; Huang, W.; Qian, Z.D. Interfacial behaviors of epoxy asphalt surfacing on steel decks. *J. Southeast Univ.* **2007**, *23*, 594–598.
16. Shen, C.J.; Tu, Z.M.; Hu, G.W.; Ou, X.M. Research on the Anticorrosion Coating Under the Paved Layer for Highway Steel Box Bridge Deck. *J. China Univ. Min. Tech.* **2006**, *16*, 429–432. [[CrossRef](#)]
17. Parhizkar, N.; Shahrabadi, T.; Ramezanzadeh, B. A new approach for enhancement of the corrosion protection properties and interfacial adhesion bonds between the epoxy coating and steel substrate through surface treatment by covalently modified amino functionalized graphene oxide film. *Corros. Sci.* **2017**, *123*, 55–75. [[CrossRef](#)]
18. Knudsen, O.; Steinsmo, U.; Bjordal, M. Zinc-rich primers-Test performance and electrochemical properties. *Prog. Org. Coat.* **2005**, *54*, 224–229. [[CrossRef](#)]
19. Bocci, E.; Canestrari, F. Analysis of Structural Compatibility at Interface between Asphalt Concrete Pavements and Orthotropic Steel Deck Surfaces. *Transp. Res. Rec.* **2012**, *2293*, 1–7. [[CrossRef](#)]

20. Jia, X.Y.; Huang, B.S.; Benjamin, F.; Tyler, B.R. Investigation of Tack Coat Failure in Orthotropic Steel Bridge Deck Overlay: Survey, Analysis, and Evaluation. *Trans. Res. Rec.* **2014**, *2444*, 28–37. [[CrossRef](#)]
21. Destrée, A.; Visscher, J.D.; Piérardand, N. Field Study to Investigate the Impact of Conditions of Application of Tack Coats on the Interlayer Bond strength. In Proceedings of the 8th RILEM International Symposium on Testing and Characterization of Sustainable and Innovative Bituminous Materials, Dresden, Germany, 7–9 October 2015; pp. 347–358.
22. Salinas, A.; Imad, L.A.; Khaled, I.H.; Ozer, H. Interface Layer Tack Coat Optimization. *Trans. Res. Rec.* **2013**, *2372*, 53–60. [[CrossRef](#)]
23. Ghumatkar, A.; Sekhar, R.; Budhe, S. Experimental study on different adherend surface roughness on the adhesive Bond strength. *Mater. Today* **2017**, *4*, 7801–7809. [[CrossRef](#)]
24. Yan, C.X.; Li, Z.G.; Su, B. Selection of Anticorrosion Adhesive Layer for Steel Deck. *Appl. Mech. Mater.* **2013**, *2547*, 361–363. [[CrossRef](#)]
25. China National Standards Commission. *Methods of Test for Drying Time of Coatings of Paints and Putties (GB/T 1728-1979)*; National Technical Committee for Standardization of Coatings and Pigments: Beijing, China, 1980. (In Chinese)
26. Local Standards of Shanxi Province. *Methods of Test for Drying Time of Coatings of Paints and Putties (GB/T1728-1979)*; Shanxi Provincial Bureau of Quality and Technical Supervision: Shanxi, China, 2012. (In Chinese)
27. *ASTM D4541-17*; Standard Test Method for Pull-Off Strength of Coatings Using Portable Adhesion Testers. ASTM International: West Conshohocken, PA, USA, 2017.
28. Xu, W.; Zhuang, G.Y.; Chen, Z.X.; Wei, J.T. Experimental Study on the Micromorphology and Strength Formation Mechanism of Epoxy Asphalt During the Curing Reaction. *Appl. Sci.* **2020**, *10*, 2610. [[CrossRef](#)]
29. Xu, W.; Wei, J.; Chen, Z.; Wang, F.; Zhao, J. Evaluation of the Effects of Filler Fineness on the Properties of an Epoxy Asphalt Mixture. *Materials* **2021**, *14*, 2003. [[CrossRef](#)] [[PubMed](#)]
30. Polaczyk, P.; Huang, B.S.; Shu, X.; Gong, H.R. Investigation into Locking Point of Asphalt Mixtures Utilizing Superpave and Marshall Compactors. *J. Mater. Civil Eng.* **2019**, *31*. [[CrossRef](#)]
31. Pang, Y.; Hao, P.W. A review of water transport in dense-graded asphalt mixtures. *Constr. Build. Mater.* **2017**, *156*, 1005–1018. [[CrossRef](#)]
32. Polaczyk, P.; Shu, X.; Gong, H.R.; Huang, B.S. Influence of aggregates angularity on the locking point of asphalt mixtures. *Road Mater. Pavement* **2019**, *20* (Suppl. 1), S183–S195. [[CrossRef](#)]
33. Zhong, K.; Xu, Y.; Wei, X.H. Investigation on surface characteristics of epoxy asphalt concrete pavement. *Int. J. Pavement Res. Tech.* **2017**, *10*, 545–552. [[CrossRef](#)]
34. Kakar, M.R.; Meor, O.H.; Jan, V. A review on moisture damages of hot and warm mix asphalt and related investigations. *J. Clean. Prod.* **2015**, *99*, 39–58. [[CrossRef](#)]
35. Ge, D.D.; You, Z.P.; Chen, S.Y.; Liu, C.C. The performance of asphalt binder with trichloroethylene: Improving the efficiency of using reclaimed asphalt pavement. *J. Clean. Prod.* **2019**, *232*, 205–212. [[CrossRef](#)]
36. Mohd, H.; Mohd, R.; You, Z.P.; David, P.; Wei, S. Laboratory moisture susceptibility evaluation of WMA under possible field conditions. *Constr. Build. Mater.* **2015**, *101*, 57–64. [[CrossRef](#)]
37. Tiankai, C.; Pan, B.F.; Sha, D.; Zhang, Y.T. Relationship between Air Voids and Permeability: Effect on Water Scouring Resistance in HMA. *J. Mater. Civil Eng.* **2021**, *33*. [[CrossRef](#)]
38. Venter, C.; Niesler, C.U. Rapid quantification of cellular proliferation and migration using Image. *J. Biotech.* **2019**, *66*, 99–102.
39. Van, D.; Abrahams, S.T.; Yilmaz, A.; Gonzalez, Y.G. Effect of surface roughness and chemistry on the adhesion and durability of a steel-epoxy adhesive interface. *Int. J. Adhes. Adhes.* **2020**, *96*, 102450.
40. Xu, J.; Cui, X.P. Robustified MANOVA with applications in detecting differentially expressed genes from oligonucleotide arrays. *Bioinformatics* **2008**, *24*, 56–62. [[CrossRef](#)] [[PubMed](#)]